WILEY | Hindawi

Research Article

A Viterbi Decoder under Class A Modeled Noise in Shallow Water

Yifei Wang [iD],[1,2,3] **Huili Fan,**[4] **Xuebo Zhang** [iD],[2,5,6] **Tian Tian,**[1,2,3] **Shaohua Hong,**[1,2,3] **Zhuofan Xie,**[1,2,3] **Ruiping Song,**[1,2,3] **Mingzhang Zhou,**[1,2,3] **Xiao Feng,**[1,2,3] **Yiting Liang,**[1] **and Shu Zhang**[4]

[1]School of Informatics, Xiamen University, Xiamen, China
[2]Key Laboratory of Southeast Coast Marine Information Intelligent Perception and Application, Ministry of Natural Resources, Xiamen, China
[3]Key Laboratory of Underwater Acoustic Communication and Marine Information Technology, Ministry of Education, Xiamen, China
[4]China Ship Development and Design Center, China
[5]College of Physics and Electronic Engineering, Northwest Normal University, Lanzhou, China
[6]Acoustic Signal & Electronics Science and Technology Corporation, Lanzhou, China

Correspondence should be addressed to Xuebo Zhang; xby_zhang@nwnu.edu.cn

A traditional Viterbi decoder is primarily optimized for additive white Gaussian noise (AWGN). With the AWGN channel, it offers good decoding performance. However, the underwater acoustic communication (UAC) channel is extremely complicated. In addition to white noise, there are a variety of artificial and natural impulse noise that occur suddenly. The traditional Viterbi decoder cannot obtain the optimum performance under this case. In order to solve this problem, this paper introduces a novel Viterbi decoder with the impulsive noise, which is considered to be subjected to Middleton Class A distribution in shallow ocean. Since Middleton Class A noise is very complicated, a simplified model is first introduced. Then, the error analysis of simplified model under various parameters is discussed in detail. The analysis shows that the simplified one just leads to slight error. Hereafter, a novel Veterbi decoder using the simplified model is discussed. Compared to a traditional decoder, a preprocessing is just required. The performance of soft decision-based decoder in the Middleton Class A noise channel (MAIN) and AWGN are further compared. Based on our simulations, the new decoder can significantly improve the performance in comparison with conventional one, which further validates our presented method.

1. Introduction

The noise distribution [1, 2] plays an important role in developing underwater signal processors. Traditional signal processors such as underwater localization [3–13], underwater tracking [9, 14, 15], sonar imaging [16–27], direction of arrival (DOA) estimation [28–32], and underwater acoustic communication (UAC) are mostly based on Gaussian noise, which can be supported by a central limit theorem. Besides, the Gaussian model is just determined by the first-order and second-order statistics [33]. Under this case, the linear processors can be obtained with Gaussian noise. Using the linear processors, the signal processing can be significantly simplified. In practice, the shallow ocean often suffers from ambient noise from shipping vessels, marine life, activity on the surrounding land, and so on. This noise is impulsive [34, 35], and it is called non-Gaussian noise [36–41], which exhibits heavier tails than the Gaussian noise. Consequently, this noise cannot be directly described by using the probability density function (PDF) of Gaussian distribution. Compared to traditional Gaussian noise, the PDF of non-Gaussian noise is extremely complicated [42–46].

Nowadays, the non-Gaussian noise [36–41, 47–49] in shallow ocean has attracted much attention in the underwater field. The related work of non-Gaussian noise, especially impulse noise, has been widely researched. The receiver

performance under different impulse noise models is also inconsistent. The duration of impulse noise is very short while its amplitude is quite high. The energy of impulse noise is almost dozens of times higher than Gaussian noise in dB. Impulse noise models can be divided into memory noise channels, such as Gilbert-Elliott channel [50] and Markov-Gaussian channel models [51–53]. GE memory impulse channel belongs to the first order two state Markov process. It assumes that the channel has one good state and one bad state. The two different states are distinguished by setting the threshold. Until now, there has been a lot of literature on the and research of Markov memory channel. For instance, the literature [51] designed a quasicyclic low-density parity-check (QC-LDPC) code to resist Markov memory impulse noise and improve the robustness. In [53], Tseng et al. added the Polar Code over Markov Gaussian memory impulse noise channels and compared the performance of SC and BP algorithms. A previous work was only Polar Code over memoryless impulse noise channels. In [54], the α-sub-Gaussian noise model with memory order m (αSGN(m)) was applied in the description of snapping shrimp noise in shallow water. The scheme tackled the optimal detection of transmitted symbols in catching shrimp noise. In this paper, we consider the impulse noise is independent of each other in the underwater acoustic channel. Therefore, we consider using the memoryless noise model.

Impulse noise also includes memoryless models such as the Gaussian Mixture Model (GMM), symmetric α-stable (SαS) distribution, and additive Middleton class A and B models. The Gaussian Mixture Model (GMM) is a parametric probability density function defined as a weighted sum of Gaussian component densities. In [55], the GMM is used to model the ocean noise, and the expectation-maximization (EM) iteration method is exploited to estimate the GMM parameters. In [56], the performance of underwater communication system in noise with GMM statistics is discussed in detail. However, the heavier tail of non-Gaussian noise cannot be comprehensively described by this statistic. To solve this problem, symmetric α-stable (SαS) distribution [57] is proposed to model the shallow ocean noise. However, this model does not have the closed-form distribution except for the Cauchy, Levy, and Gaussian distributions. This is not convenient for the performance analysis of signal processors. In addition, Middleton class A noise has a strict probability density function(PDF) which simplifies the algorithmic complexity. The major advantage is that Middleton class A noise is a generalized GMM model. We can adjust the parameters of Middleton Class A impulse noise models to fit the underwater acoustic environment.

Actually, traditional processors are often discussed based on the empirical non-Gaussian models. To some degree, the statistics of ocean ambient noise are just fitted by using empirical non-Gaussian models, and the parameters of non-Gaussian noise model do not have physical meaning. Based on the physical mechanism of noise source and noise propagation characteristic, Middleton noise [58] possessing physical meaning is proposed. In [39], a parameter estimation method based on characteristic function for the Middleton Class A model is presented. In [38], the parameter

estimation of Middleton Class B noise is discussed based on the least-square estimation method. In [59], the mixture noise including $\widehat{SI} \pm S$ distribution and Gaussian distribution is discussed. In practice, their model is a simplification of Middleton Class B model. In general, Middleton Class A is a general GMM model. Compare to the Class A model, the Class B model is very complicated. In this paper, we mainly concentrate on the Viterbi decoder and its performance with the Middleton Class A model.

The remainder of this work is arranged in the following. Section 2 introduces the PDF of Middleton Class A model and simplified one. In Section 3, the convolutional code and Viterbi decoder are presented. Then, the performance of the Viterbi decoder with Class A model is discussed in detail. Lastly, some conclusions are reported in the last section.

2. Middleton Class A Impulsive Model

In this section, an impulsive noise model named Middleton Class A is introduced.

2.1. The PDF of the Middleton Class A Noise. The one-dimensional PDF of normalized Middleton's Class A noise model can be expressed as

$$f_{A,\Gamma}(n) = \sum_{m=0}^{\infty} C_m \cdot \frac{1}{\sqrt{2\pi\sigma_m^2}} \exp\left(-\frac{n^2}{2\sigma_m^2}\right), \quad (1)$$

$$C_m = \frac{e^{-A}A^m}{m!}, \quad (2)$$

where the impulse index A is the product of the average number of pulses received per unit time and the pulse duration. It determines that the noise can be arbitrarily close to Gaussian noise and the Poisson process. The Gaussian coefficient Γ is the ratio of the average power of the Gaussian noise to the average power of the impulse noise. It is defined as

$$\Gamma = \frac{\sigma_G^2}{\sigma_I^2}, \quad (3)$$

where the receiver variance $0, 0, 1\,\sigma_m^2$ can be described by

$$\sigma_m^2 = \sigma_G^2 + \sigma_I^2 \frac{m}{A} = \sigma^2 \frac{m/A + \Gamma}{1 + \Gamma}. \quad (4)$$

The total noise variance of the receiver σ^2 can be calculated as

$$\sigma^2 = \sigma_G^2 + \sigma_I^2. \quad (5)$$

The PDF of Class A noise is the sum of numerous zero-mean Gaussian PDFs with different weights. As shown by Equation (1), the noise source distribution obeys the Poisson distribution. In general, the impulse of noise is influenced by A and Γ. The Middleton Class A noise model is very close to Gaussian noise when the values of A and Γ are relatively large. The impulse of noise will
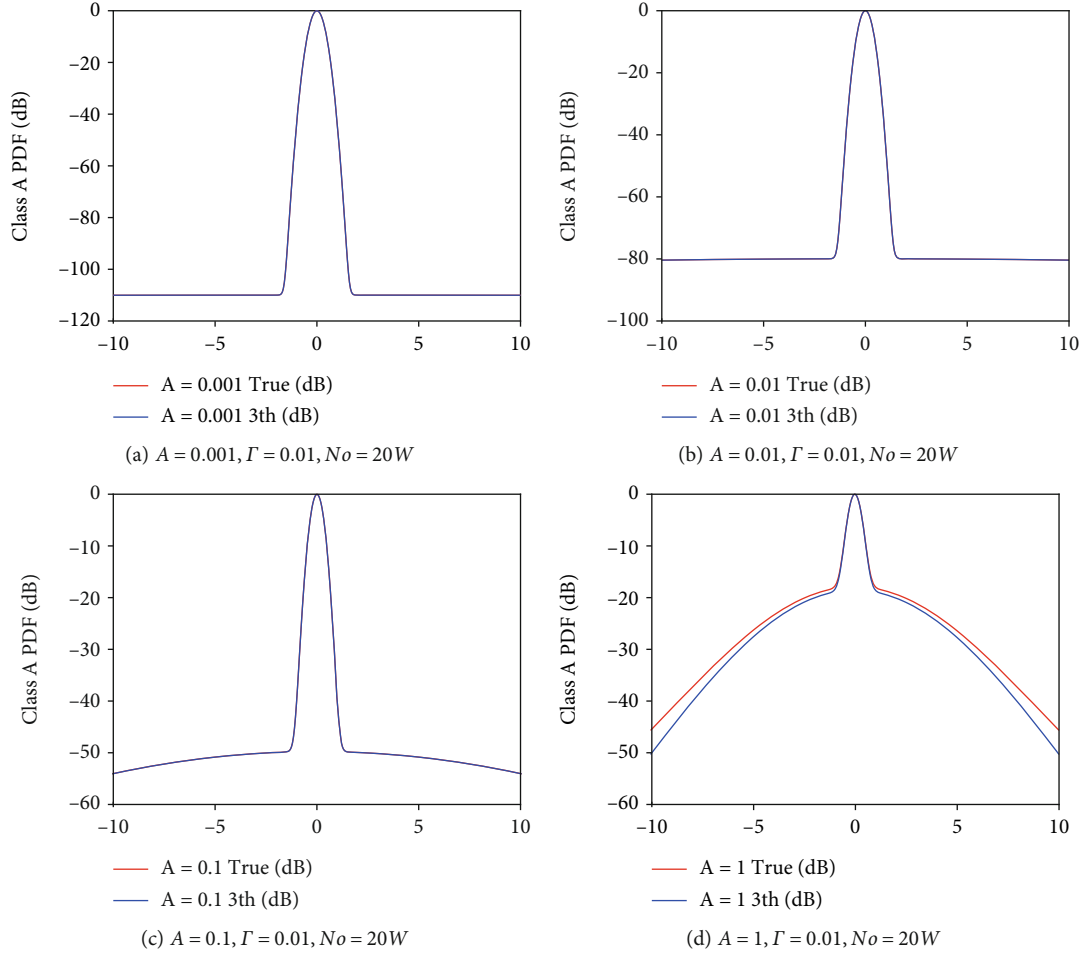
FIGURE 1: PDF of Middleton Class A with the different parameter A ($\Gamma = 0.01, No = 20W$).

(a) $A = 0.001, \Gamma = 0.01, No = 20W$

(b) $A = 0.01, \Gamma = 0.01, No = 20W$

(c) $A = 0.1, \Gamma = 0.01, No = 20W$

(d) $A = 1, \Gamma = 0.01, No = 20W$

become stronger as A and Γ decrease. Thus, the total noise interference can be influenced through A and Γ.

2.2. The Error Analysis of Truncated Model of Class A Noise. Since the PDF of Class A noise consists of infinite series, it is undesirable in reality. We explore the truncation model for Class A noise. Experiments indicate that the finite terms of noise can be adopted when A is small enough [60].

A truncation to the first three terms of the PDF is as follows:

$$\widehat{f}_{A,\Gamma}(n) = \sum_{m=0}^{2} C_m \cdot \frac{1}{\sqrt{2\pi\sigma_m^2}} \exp\left(-\frac{n^2}{2\sigma_m^2}\right). \quad (6)$$

The impact of parameters A, Γ, and No on the PDF between the simplified model and true one (Approximate replacement of the first 300,000 terms) is then discussed.

2.2.1. Error Analysis with Different Parameter A. Before discussion, we need to normalize the probability density function and then take the logarithm.

When $\Gamma = 0.01$, $No = 20W$, and $A = [0.001\ 0.01\ 0.1\ 1]$, respectively, the error between the simplified model and the true one of the Class A noise PDF is discussed in Figure 1.

As depicted in Figure 1, the order m of the Middleton Class A noise approximate model is related to A. When A is small enough, the error of the approximation model in Equation (6) is close to 0. When A is in the range from 0.1 to 1, the simplified model can not be a good substitution. The reason is owed to the impulsive weakening of non-Gaussian noise, bringing it closer to Gaussian noise.

2.2.2. Error Analysis with Different Parameter Γ. When $\Gamma = [0.001\ 0.01\ 0.1\ 1]$, the error between the simplified model and the true one of Class A noise PDF is shown in Figures 2–4. In the simulations, No is set to $20W$, and A is $[0.001\ 0.01\ 0.1\ 1]$.

By comparing Figures 2–4, it can be observed that the value of Γ has no effect on the error of the PDF approximate model in Middleton Class A noise.

2.2.3. Error Analysis with Different Parameter No. In this subsection, the differences between the simplified model and the true model of the Class A noise PDF will be discussed. The results are exhibited in Figure 5, where $\Gamma = 0.01$, $No = [20\ 2\ 0.2]$, and $A = 0.01$.

In Figure 5, note that the error of the PDF simplified model has nothing to do with the parameter No. When No takes different values, the error is always around 0.

(a) $A = 0.01, \Gamma = 0.001, No = 20W$

(b) $A = 0.01, \Gamma = 0.01, No = 20W$

(c) $A = 0.01, \Gamma = 0.1, No = 20W$

(d) $A = 0.01, \Gamma = 1, No = 20W$
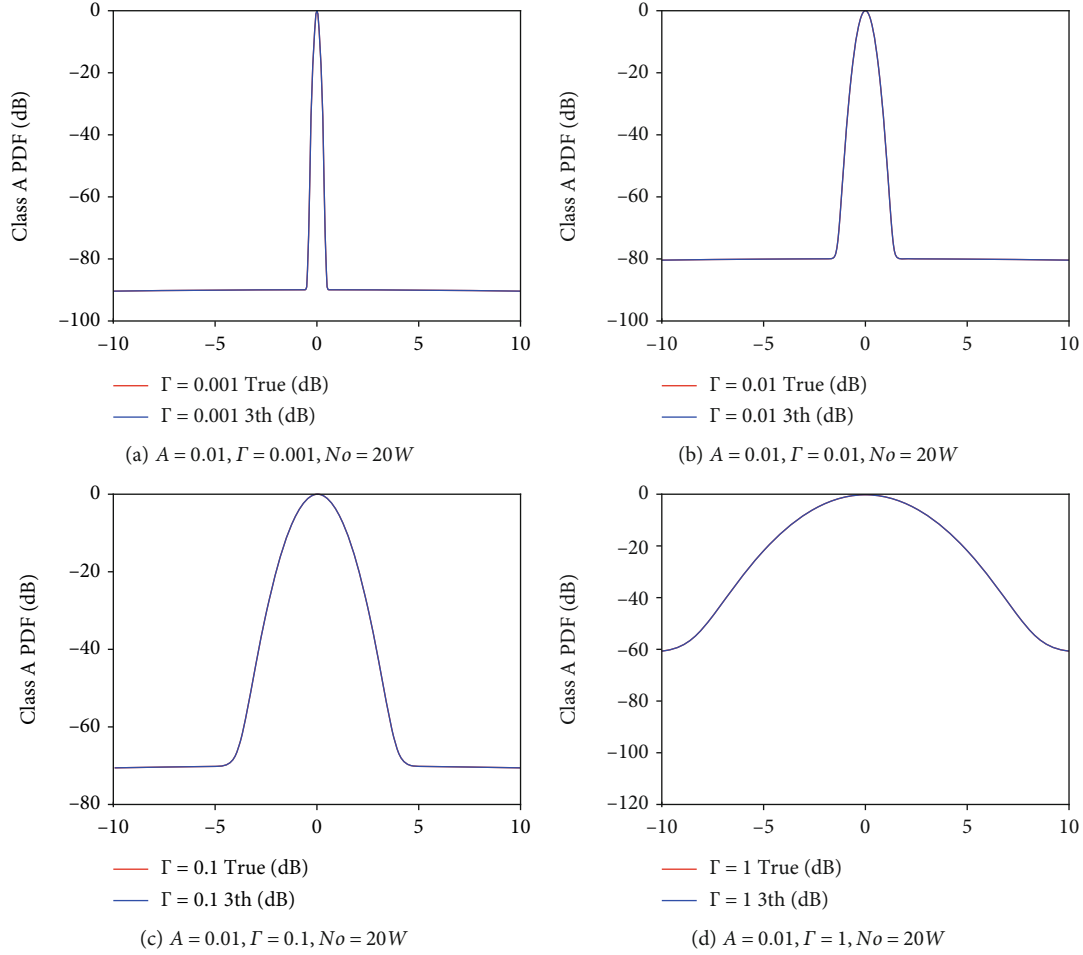
FIGURE 2: PDF of Middleton Class A with the different parameter Γ ($A = 0.01, No = 20W$).

3. Convolutional Code and Viterbi Decoding

Convolutional coding is a very promising coding technique proposed by Elias et al. in 1955. It has been widely used in communication systems, especially in satellite communication systems. Among them, the Odenwalder convolutional coding with code rates of 1/2 and 1/3 and constraint length $K = 7$ has become the standard coding method in commercial satellite communication systems. In 1967, Viterbi proposed a probabilistic decoding algorithm for convolutional encoding—the Viterbi algorithm. When the constraint degree of the code is small, it is more efficient and faster than other probabilistic decoding algorithms. Besides, the decoder is simpler. Since the Viterbi algorithm was proposed, it has been developed quickly in both theory and practice. The Viterbi algorithm has been widely used in various digital communication systems.

3.1. Generation of Convolutional Code. Convolutional code is a channel code with error correction capability, which can effectively reduce transmission error [61]. The decoding method is Viterbi decoding. Convolutional code can be described by (n, k, L). In this way, n represents the code length corresponding to the output of the encoder. k is the length of the effective information group, which is the input

of the encoder. L denotes the constraint length. The code rate of the convolutional code is k/n. The n bits of the encoding output not only depend on the k bits but also depend on the $k - 1$ bit input before this. So the convolutional encoder has the property of "memory."

Take $(2, 1, 3)$ convolutional code as an example.

By using the delay factor, the information sequence $M_0 M_1 M_2 \cdots M_{l-1}$ and convolutional code series $C_0 C_1 C_2 \cdots C_{l-1}$ can be described by

$$a_i = M_i \oplus M_{i-1} \oplus M_{i-2}, \quad 0 \le i \le l - 1, \tag{7}$$

$$b_i = M_i \oplus M_{i-2}, \quad 0 \le i \le l - 1. \tag{8}$$

$$\mathbf{C_i} = \mathbf{a_i b_i}, \tag{9}$$

where M_i is current input information bit and M_{i-1} and M_{i-2} are the first and the first two information bits. When $i \le 0, M_i = 0$, set the initial state of the delay register to 0.

The generator polynomial of the Convolutional code is expressed as

$$G(Z) = \left[1 + Z^{-1} + Z^{-2} \ 1 + Z^{-2} \right], \tag{10}$$

where Z represents delay register.

(a) $A = 0.1, \Gamma = 0.001, No = 20W$

(b) $A = 0.1, \Gamma = 0.01, No = 20W$

(c) $A = 0.1, \Gamma = 0.1, No = 20W$

(d) $A = 0.1, \Gamma = 1, No = 20W$
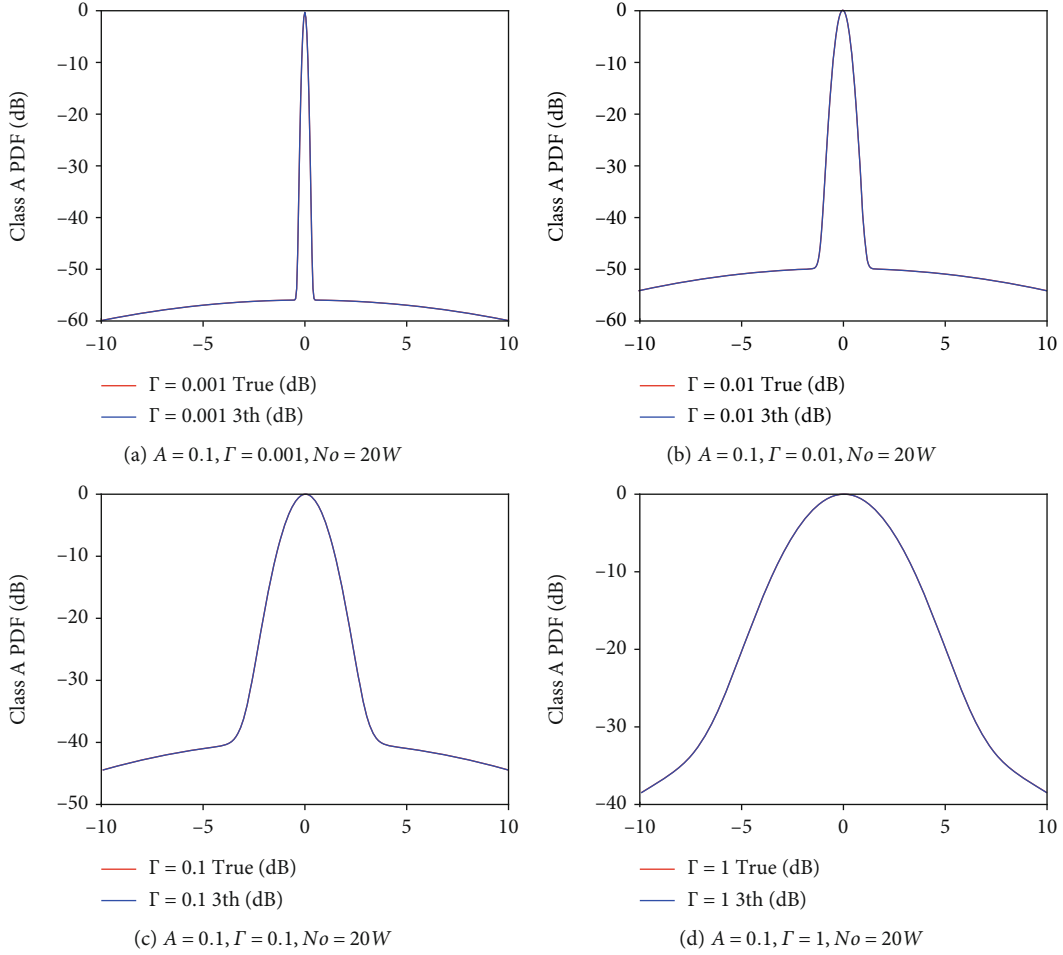
FIGURE 3: PDF of Middleton Class A with the different parameter Γ ($A = 0.1, No = 20W$).

3.2. Trellis Diagram.

Trellis graphs are used in the Viterbi decoding. It cannot be a representation of a single state. The trellis graphs are joined in a chronological sequence to define the relationship between time and state transition, generating a network of convolutional codes. The encoding process of the convolutional encoder is dynamic.

The following are the important concepts in the trellis diagram:

(i) Calculate the branch metric (BM)

Calculate the Hamming distance (hard decision) or Euclidean distance (soft decision) between the input symbol and the output symbol corresponding to two paths, which is the branch metric of two paths.

(ii) Calculate the path metric (PM)

To obtain the two metrics at time t, the BM of the two pathways is added to the state metrics recorded in the appropriate state at time $t - 1$.

(iii) Select the surviving path

Compare the path metrics and maintain the smallest one as the state metric at time t, as well as the formation path.

(iv) Traceback depth

Generally, the Viterbi decoder's backtracking depth is 6 times the constraint length. Set the traceback depth to 18 in this document.

In Figure 6, the uncoded sequence is $\mathbf{M} = M_0 M_1 M_2 \cdots M_{l-1}$. The output sequence of convolutional code is $\mathbf{C} = C_0 C_1 C_2 \cdots C_{l-1}$. Assume that the sequence after binary modulation is $\mathbf{V} = V_0 V_1 V_2 \cdots V_{l-1}$ and the channel output sequence is $\mathbf{R} = R_0 R_1 R_2 \cdots R_{l-1}$. The decoder must generate an estimate of the code sequence $\hat{\mathbf{V}}$ based on the accepted sequence $\mathbf{R}$. The maximum likelihood decoding is to choose maximize the log likelihood function $\log P(r|c)$ as $\hat{\mathbf{V}}$.

$$P(r|v) = \prod_{l=0}^{N-1} P(r_l|v_l). \tag{11}$$

Hence,

$$\log P(r|v) = \sum_{l=0}^{N-1} \log P(r_l|v_l), \tag{12}$$

where $P(r_l|v_l)$ is the channel transition probability. Log-

(a) $A = 1, \Gamma = 0.001, No = 20W$

(b) $A = 1, \Gamma = 0.01, No = 20W$

(c) $A = 1, \Gamma = 0.1, No = 20W$

(d) $A = 1, \Gamma = 1, No = 20W$
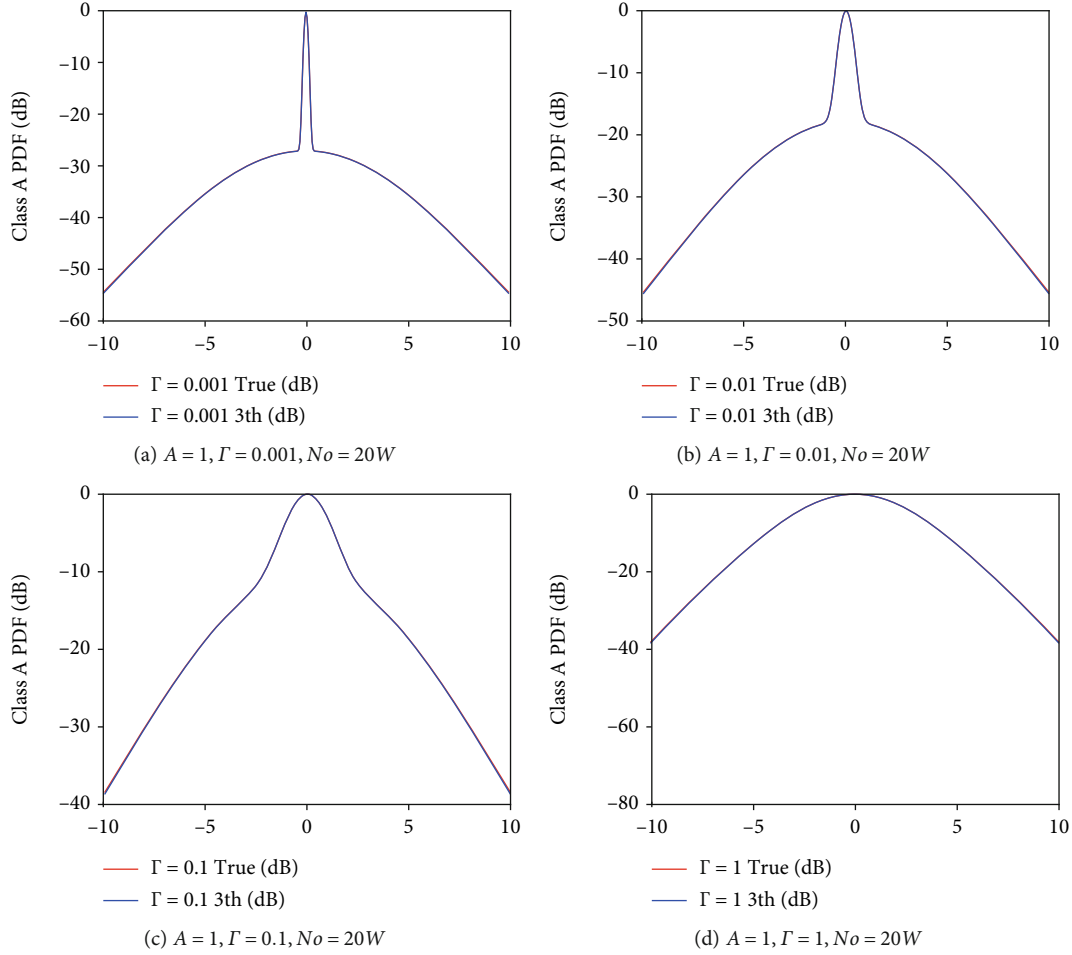
FIGURE 4: PDF of Middleton Class A with the different parameter Γ ($A = 1, No = 20W$).

likelihood function $\log P(r|v)$ is the metric of **C**, where $\log P(r_l|v_l)$ is called the branch metric.

4. Performance of Viterbi Decoder under Class A Noise

The system block diagram and bit error rate formula under BPSK modulation are presented in this section. In addition, we pay specific attention to the effect on the best receivers after the Class A noise channel.

The full simulation system is presented in Figure 7.

As a soft decision symbol, the log-likelihood ratio is introduced to the Viterbi decoder input [62].

$$\text{LLR} = \ln f_{A,\Gamma}\left(r_l - \sqrt{E_b}\right) - \ln f_{A,\Gamma}\left(r_l + \sqrt{E_b}\right). \quad (13)$$

We first introduce the branch metric and LLR formula of Viterbi decoding under the Gaussian channel.

In BPSK modulation, we use the bit energy E_b to normalize the Gaussian pdf, where the mapping rule $1 \longrightarrow +\sqrt{E_b}$, $1 \longrightarrow -\sqrt{E_b}$. Denote $E_b = v_l^2$ and $N_G = 2\sigma^2$ as bit energy and total noise power, respectively. The code rate of convolutional code is $R_c = 1/2$. We consider the value of ± 1

sequence $\mathbf{V} = V_0 V_1 V_2 \cdots V_{l-1}$ and accepted sequence $\mathbf{R} = R_0 R_1 R_2 \cdots R_{l-1}$.

The PDF of Gaussian noise can be expressed as

$$P_G(n) = \frac{1}{\sqrt{2\pi}\sigma} \exp\left(-\frac{n^2}{2\sigma^2}\right). \quad (14)$$

The branch metric and LLR under the traditional Gaussian decoder can be expressed as

$$\mathbf{r} \times \mathbf{v} = \sum_{l=0}^{N-1} r_l \cdot v_l, \quad (15)$$

$$L(y_k) = \frac{2}{\sigma_G^2} y_k. \quad (16)$$

The bit error rate formula under the influence of Gaussian noise can be written as

$$\text{BER}_{\text{AWGN}} = \frac{1}{2} \operatorname{erf} c\left(\sqrt{\frac{E_b}{N_G}}\right). \quad (17)$$

The PDF of Class A noise consists of infinite terms,

(a) $A = 0.01, \Gamma = 0.01, No = 20W$

(b) $A = 0.01, \Gamma = 0.01, No = 2W$

(c) $A = 0.01, \Gamma = 0.01, No = 0.2W$
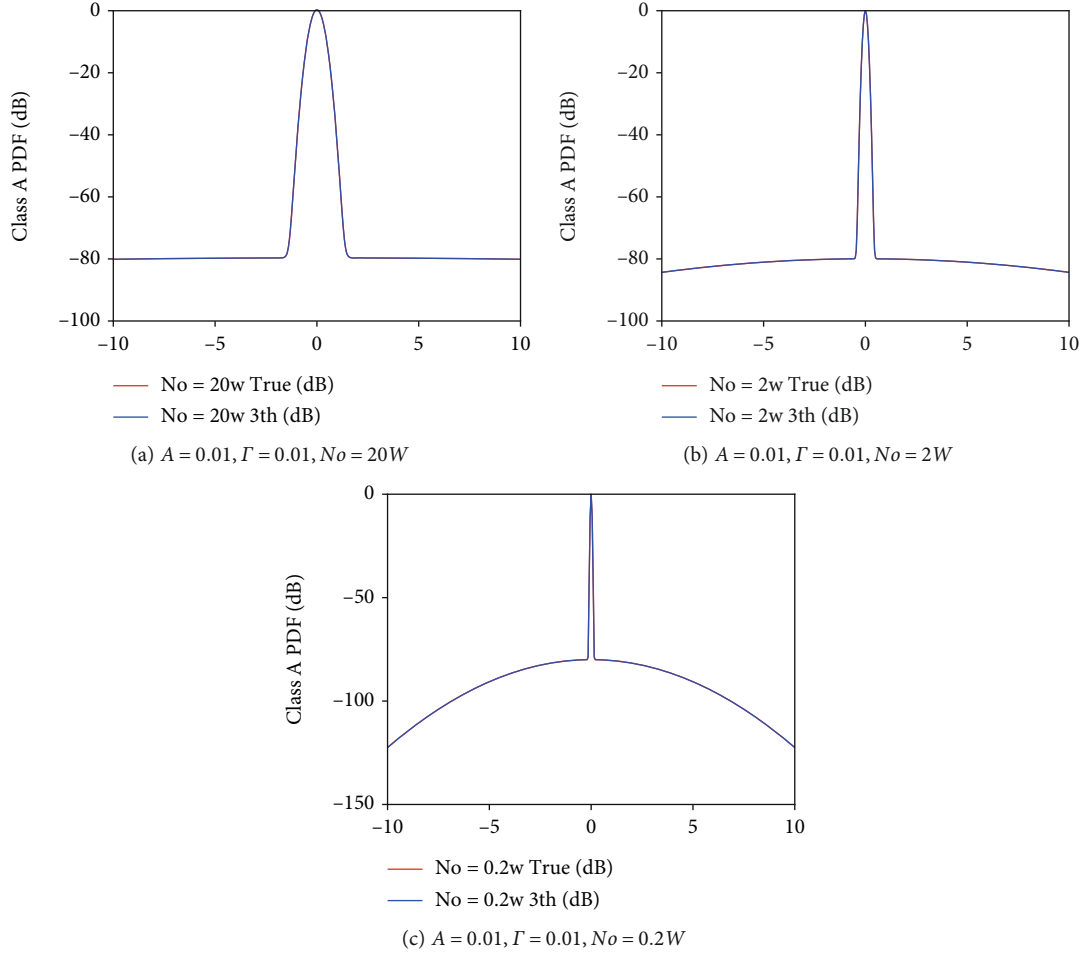
FIGURE 5: PDF of Middleton Class A with the different parameter No ($A = 0.01, \Gamma = 0.01$).
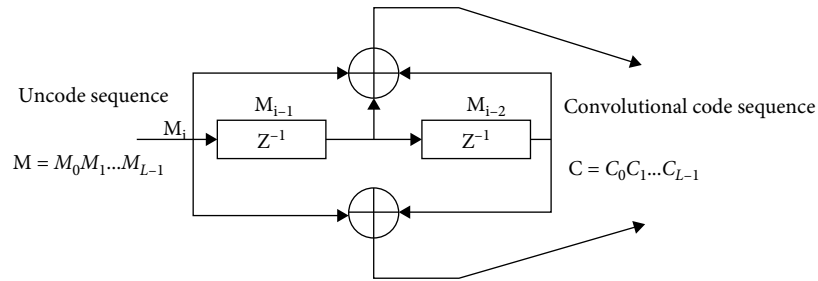
FIGURE 6: (2, 1, 3) convolutional encoder.

leading to the enormous complexity of logarithmic. We use the 3-order approximate model and Equation (13) to simplify the soft symbol.

$$\ln \widehat{f}_{A,\Gamma}(n) = \ln_{\max_{m=0,1,2}} \frac{\left[C_m \cdot \left(1/\sqrt{2\pi}\sigma_m \right) e^{\left(-\left(r_i - \sqrt{E_b} \right)^2 \right)/2\sigma_m^2} \right]}{\left[C_m \cdot \left(1/\sqrt{2\pi}\sigma_m \right) e^{\left(-\left(r_i + \sqrt{E_b} \right)^2 \right)/2\sigma_m^2} \right]}.$$

(18)

The Class A noise Viterbi decoder can be established by

Equation (13). The algorithm equation can be depicted as soft decision based on Class A noise PDF simplified model, as shown in Equation (18).

The bit error rate formula under the influence of Class A noise can be obtained as

$$\mathrm{BER}_{\mathrm{MAIN}} = \frac{1}{2} \sum_{m=0}^{+\infty} \frac{e^{-A} A^m}{m!} \, \mathrm{erf} \, c\left(\sqrt{\frac{A\Gamma + A}{A\Gamma + m} \frac{E_b}{N_0}} \right). \quad (19)$$

When A is very small, we take the first 3 orders as an approximation
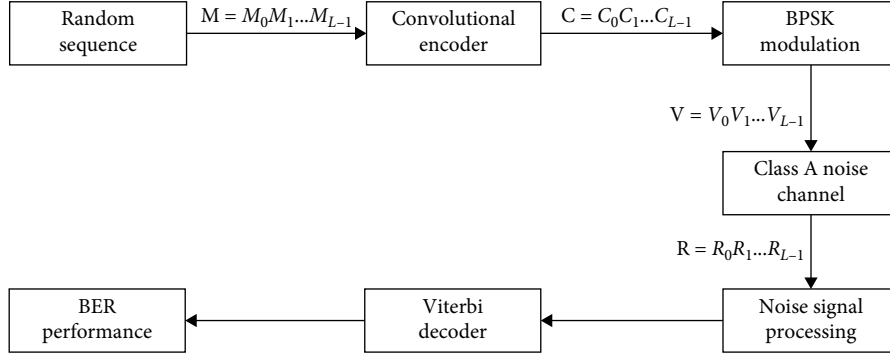
FIGURE 7: Block diagram of signal processing.
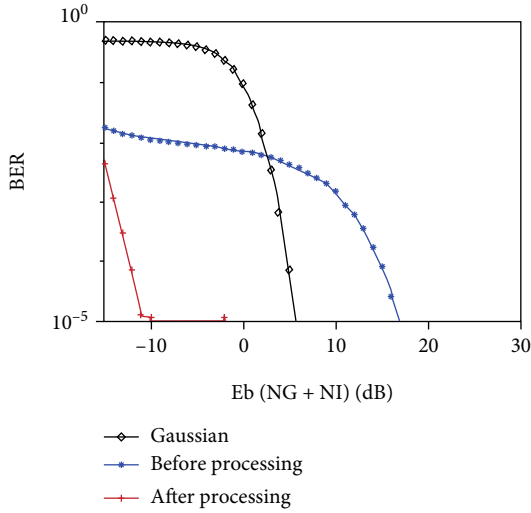
FIGURE 8: BER performance soft decision before and after processing ($A = 0.01, \Gamma = 0.01$).
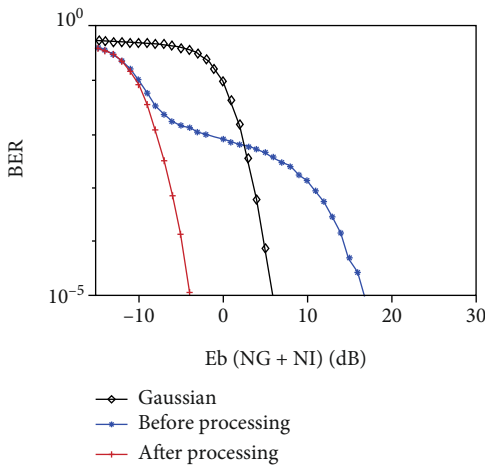
FIGURE 9: BER performance soft decision before and after processing ($A = 0.01, \Gamma = 0.1$).

$$\text{BER}_{\text{MAIN}} = \frac{1}{2} \sum_{m=0}^{2} \frac{e^{-A} A^m}{m!} \text{ erf } c \left(\sqrt{\frac{A\Gamma + A}{A\Gamma + m} \frac{E_b}{N_0}} \right). \qquad (20)$$

Finally, based on our simplified model, we present the soft decision of BER performance in the proposed decoder after signal processing Middleton Class A noise under different parameters.

According to Figure 8, the proposed decoder outperforms the signal processing of soft decision in the Class A noise channel. It is worth noting that when the noise has a higher impulse, the BER performance improves significantly. When the BER approaches 10^{-5}, the gain of $A = 0.01$ and $\Gamma = 0.01$ is around 25-30 dB. As shown in Figure 9, the gain of $A = 0.01$ and $\Gamma = 0.1$ is only 20 dB, which is owing to the noise trending to Gaussian noise at this time. It can be seen that the coefficient of the Gaussian Γ will also affect the performance of the decoder.

5. Conclusion

In this paper, a method of processing Middleton Class A noise by the Viterbi decoder is introduced in the field of shallow water acoustic communication. The effects of the three parameters A, No, and Γ of Middleton class A noise on the third-order approximate model are also investigated. It can be concluded that parameters No and Γ just influence the curve's shape but have no effect on the third-order approximate model, while parameter A influences the approximate model. When A is less than 0.1, the third-order model can be a good approximation to replace the real model in the curve of probability density probability. At the same time, the BER performance in the final section proves its feasibility under various parameters.

Additionally, the Class A noise decoder's system block diagram is constructed in the paper. The noise processing algorithm is derived from the optimum reception theory of Class A noise. After signal processing, the decoder overcomes the drawbacks of traditional decoders in Class A noise channel reception and enhances soft decision performance.

Data Availability

The data used to support the findings of this study were supplied by Yifei Wang under license and so cannot be made freely available. Requests for access to these data should be made to Yifei Wang (23320201154028@stu.xmu.edu.cn).

Conflicts of Interest

The authors declare no conflicts of interest.

Acknowledgments

References

[1] H. Paik, N. Sastry, and I. SantiPrabha, "Effectiveness of noise jamming with white Gaussian noise and phase noise in amplitude comparison monopulse radar receivers," in *2014 IEEE International Conference on Electronics, Computing and Communication Technologies (CONECCT)*, pp. 1–5, Bangalore, India, 2014.

[2] S. V. Uppala and J. D. Sahr, "Computing probability of errors of linear multiuser detectors in white Gaussian noise and Rayleigh fading channels," in *ICC '98. 1998 IEEE International Conference on Communications. Conference Record. Affiliated with SUPERCOMM'98 (Cat. No.98CH36220)*, vol. 1, pp. 360–364, Atlanta, GA, USA, 1998.

[3] J. Kim, "3D path planner of an autonomous underwater vehicle to track an emitter using frequency and azimuth–elevation angle measurements," *IET Radar, Sonar & Navigation*, vol. 14, no. 8, pp. 1236–1243, 2020.

[4] X. Zhang, J. Tang, F. Wang, S. Bai, and D. Liu, "Accurate back projection imaging algorithm for multi-receiver SAS in engineering application," *Journal of Naval University of Engineering*, vol. 26, no. 2, pp. 20–24, 2014.

[5] C. Zhao, W. Zhu, G. Qiao, and F. Zhou, "Optimisation method with node selection and centroid algorithm in underwater received signal strength localisation," *IET Radar, Sonar & Navigation*, vol. 14, no. 11, pp. 1681–1689, 2020.

[6] X. Zhang, J. Tang, and J. Ouyang, "Imaging processor for multi-receiver sas in the presence of partially failed receivers," *Applied Mechanics and Materials*, vol. 543-547, no. 2, pp. 2225–2228, 2014.

[7] X. Zhang, W. Ying, and Y. Liu, "Processing multireceiver SAS data based on the PTRS linearization," in *2021 IEEE International Geoscience and Remote Sensing Symposium (IGARSS)*, pp. 5167–5170, Brussels, Belgium, 2021.

[8] B. Zhu, D. Li, Z. Li, H. He, and X. Li, "Robust adaptive Kalman filter for strapdown inertial navigation system dynamic alignment," *IET Radar, Sonar & Navigation*, vol. 15, no. 12, pp. 1583–1593, 2021.

[9] X. Zhang, P. Yang, and X. Dai, "Focusing multireceiver SAS data based on the fourth-order legendre expansion," *Circuits, Systems, and Signal Processing*, vol. 38, no. 6, pp. 2607–2629, 2019.

[10] C. Wang, B. Wang, Z. Ding, and M. Fu, "A co-occurrence matrix-based matching area selection algorithm for underwater gravity-aided inertial navigation," *IET Radar, Sonar & Navigation*, vol. 15, no. 3, pp. 250–260, 2021.

[11] C. Tan, X. Zhang, P. Yang, and M. Sun, "A novel sub-bottom profiler and signal processor," *Sensors*, vol. 19, no. 22, p. 5052, 2019.

[12] H. Li, A. Jakobsson, D. Sun, and C. Zheng, "Underwater source localization in the presence of strong interference," *IET Radar, Sonar & Navigation*, vol. 15, no. 3, pp. 226–239, 2021.

[13] X. Zhang, P. Yang, and M. Sun, "Experiment results of a novel sub-bottom profiler using synthetic aperture technique," *Current Science*, vol. 122, no. 4, pp. 461–464, 2022.

[14] H. Son, "Smart tracking algorithm for multi-static sonar based on expectation maximisation," *IET Radar, Sonar & Navigation*, vol. 14, no. 10, pp. 1624–1630, 2020.

[15] J. Kim, "Filter re-start strategy for angle-only tracking of a highly manoeuvrable target considering the target's destination information," *IET Radar, Sonar & Navigation*, vol. 14, no. 6, pp. 935–943, 2020.

[16] G. Delyon, "Clutter map detector for active diver detection sonar," *IET Radar, Sonar & Navigation*, vol. 14, no. 1, pp. 177–186, 2020.

[17] X. Zhang, H. Wu, H. Sun, and W. Ying, "Multireceiver sas imagery based on monostatic conversion," *IEEE Journal of Selected Topics in Applied Earth Observations and Remote Sensing*, vol. 14, pp. 10835–10853, 2021.

[18] X. Zhang, X. Dai, and B. Yang, "Fast imaging algorithm for the multiple receiver synthetic aperture sonars," *IET Radar, Sonar & Navigation*, vol. 12, no. 11, pp. 1276–1284, 2018.

[19] M. Rashed, M. Meijer, and P. Teal, "Performance of the matched filter in sonar systems having time variable gain," *IET Radar, Sonar & Navigation*, vol. 14, no. 3, pp. 425–430, 2020.

[20] X. Zhang, J. Tang, H. Zhong, and S. Zhang, "Wavenumber-domain imaging algorithm for wide-beam multi-receiver synthetic aperture sonar," *Journal of Harbin Engineering University*, vol. 35, no. 1, pp. 93–101, 2014.

[21] X. Zhang, C. Tan, and W. Ying, "An imaging algorithm for multireceiver synthetic aperture sonar," *Remote Sensing*, vol. 11, no. 6, p. 672, 2019.

[22] J. Mei, Y. Pei, Y. Zakharov, D. Sun, and C. Ma, "Improved underwater acoustic imaging with non-uniform spatial resampling RL deconvolution," *IET Radar, Sonar & Navigation*, vol. 14, no. 11, pp. 1697–1707, 2020.

[23] X. Zhang and P. Yang, "Imaging algorithm for multireceiver synthetic aperture sonar," *Journal of Electrical Engineering and Technology*, vol. 14, no. 1, pp. 471–478, 2019.

[24] X. Zhang and P. Yang, "An improved imaging algorithm for multi-receiver sas system with wide-bandwidth signal," *Remote Sensing*, vol. 13, no. 24, p. 5008, 2021.

[25] D. Gillis, "An underwater target detection framework for hyperspectral imagery," *IEEE Journal of Selected Topics in Applied Earth Observations and Remote Sensing*, vol. 13, pp. 1798–1810, 2020.

[26] X. Zhang, P. Yang, P. Huang, H. Sun, and W. Ying, "Wide-bandwidth signal-based multireceiver SAS imagery using extended chirp scaling algorithm," *IET Radar, Sonar & Navigation*, vol. 16, no. 3, pp. 531–541, 2022.

[27] Y. Xie, N. Bore, and J. Folkesson, "Inferring depth contours from sidescan sonar using convolutional neural nets," *IET Radar, Sonar & Navigation*, vol. 14, no. 2, pp. 328–334, 2020.

[28] X. Zhang and W. Ying, "Influence of the element beam pattern on synthetic aperture sonar imaging," *Geomatics and Information Science of Wuhan University*, vol. 47, no. 1, pp. 133–140, 2022.

[29] F. Jiang, Z. Zhao, H. Najafabadi, and Y. Yang, "Underwater TDOA/FDOA joint localisation method based on cross-

ambiguity function," *IET Radar, Sonar & Navigation*, vol. 14, no. 8, pp. 1256–1266, 2020.

[30] X. Zhang, X. Dai, and B. Fang, "An imaging Algorithm for multireceiver synthetic aperture sonar," *Geomatics and Information Science of Wuhan University*, vol. 11, no. 6, pp. 672–1673, 2019.

[31] M. Rajan and A. Mohanty, "Time delay estimation using wavelet denoising maximum likelihood method for underwater reverberant environment," *IET Radar, Sonar & Navigation*, vol. 14, no. 8, pp. 1183–1191, 2020.

[32] R. Naus and Y. Toh, "Time difference of arrival localisation exploiting all available time differences," *IET Radar, Sonar & Navigation*, vol. 14, no. 2, pp. 252–256, 2020.

[33] A. Tollkuhn, F. Particke, and J. Thielecke, "Gaussian state estimation with non-gaussian measurement noise," in *2018 Sensor data fusion: trends, solutions, applications (SDF)*, pp. 1–5, Bonn, Germany, 2018.

[34] M. Chunxia, S. Dan, C. Feng, Z. Xuegang, H. Jing, and B. Jin, "Statistical characteristic of spectrum for ambient noise at high frequencies in shallow water," in *2017 IEEE International Conference on Signal Processing, Communications and Computing (ICSPCC)*, pp. 1–4, Xiamen, China, 2017.

[35] S. Kassam, *Signal Detection in Non-Gaussian Noise*, Springer Science & Business Media, 2012.

[36] Y. Fangyuan, Q. Guo, and D. Li, "Performance of iterative ofdm receiver in doubly spread underwater acoustic communication channel," in *2014 12th International Conference on Signal Processing (ICSP)*, pp. 1579–1583, Hangzhou, China, 2014.

[37] I. Prokopenko and N. Babanska, "Detection algorithm of non-Gaussian character of sample 1 distribution and its implementation in radar data processing," in *2015 Signal Processing Symposium (SPSympo)*, pp. 1–4, Debe, Poland, 2015.

[38] X. Zhang, W. Ying, P. Yang, and M. Sun, "Parameter estimation of underwater impulsive noise with the class B model," *IET Radar, Sonar & Navigation*, vol. 14, no. 7, pp. 1055–1060, 2020.

[39] X. Zhang, W. Ying, and B. Yang, "Parameter estimation for class a modeled ocean ambient noise," *Journal of Engineering and Technological Sciences*, vol. 50, no. 3, pp. 330–345, 2018.

[40] X. Zhang, C. Tan, and W. Ying, "Characteristic function based parameter estimation for ocean ambient noise," in *2018 IEEE 3rd International Conference on Image, Vision and Computing (ICIVC)*, pp. 817–820, Chongqing, China, 2018.

[41] S. Banerjee and M. Agrawal, "Underwater acoustic communication in the presence of heavytailed impulsive noise with biparameter cauchyGaussian mixture model," in *2013 Ocean Electronics (SYMPOL)*, pp. 1–7, Kochi, India, 2013.

[42] N. Guney, H. Delic, and M. Koca, "Robust detection of ultrawideband signals in non-Gaussian noise," *IEEE Transactions on Microwave Theory and Techniques*, vol. 54, no. 4, pp. 1724–1730, 2006.

[43] G. Guo, M. Mandal, and Y. Jing, "A robust detector of known signal in non-Gaussian noise using threshold systems," *Signal Processing*, vol. 92, no. 11, pp. 2676–2688, 2012.

[44] F. Duan, F. Chapeau-Blondeau, and D. Abbott, "Non-Gaussian noise benefits for coherent detection of narrowband weak signal," *Physics Letters A*, vol. 378, no. 26-27, pp. 1820–1824, 2014.

[45] V. Hari, G. Anand, A. Premkumar, and A. Madhukumar, "Design and performance analysis of a signal detector based on suprathreshold stochastic resonance," *Signal Processing*, vol. 92, no. 7, pp. 1745–1757, 2012.

[46] D. Rousseau, G. Anand, and F. Chapeau-Blondeau, "Noise-enhanced nonlinear detector to improve signal detection in non-Gaussian noise," *Signal Processing*, vol. 86, no. 11, pp. 3456–3465, 2006.

[47] S. Yang, Y. Yang, and Y. Ma, "Investigation of the horizontal directivity of underwater ambient noise with the circular hydrophone array," *The Journal of the Acoustical Society of America*, vol. 131, no. 4, pp. 3484–3484, 2012.

[48] P. Akimov, P. Bakut, and V. Bogdanovich, *Theory of Signal Detection*, vol. 440, Radio i svyaz, Moscow, 1984.

[49] W. Ying, P. Yang, C. Li, and J. Liu, "A comparison between two parameter estimation methods for non-Gaussian noise models," in *2020 IEEE 5th International Conference on Signal and Image Processing (ICSIP)*, pp. 623–627, Nanjing, China, 2020.

[50] T. Farjam, T. Charalambous, and H. Wymeersch, "Timer-based distributed channel access in networked control systems over known and unknown Gilbert-Elliott channels," in *2019 18th European Control Conference (ECC)*, pp. 2983–2989, Naples, Italy, 2019.

[51] D.-F. Tseng and S.-S. Lin, "Robust low density parity check decoding over markov gaussian channels," in *2019 IEEE 89th Vehicular Technology Conference (VTC2019-Spring)*, pp. 1–5, Kuala Lumpur, Malaysia, 2019.

[52] D.-F. Tseng, F. G. Mengistu, Y. S. Han, M. Abera Mulatu, L.-C. Chang, and T.-R. Tsai, "Robust turbo decoding in a Markov Gaussian channel," *IEEE Wireless Communications Letters*, vol. 3, no. 6, pp. 633–636, 2014.

[53] S.-M. Tseng, W.-C. Hsu, and D.-F. Tseng, "Deep learning based decoding for polar codes in Markov Gaussian memory impulse noise channels," *Wireless Personal Communications*, vol. 122, no. 1, pp. 737–753, 2022.

[54] A. Mahmood and M. Chitre, "Viterbi detection of psk signals in markov impulsive noise," in *2018 OCEANS - MTS/IEEE Kobe Techno-Oceans (OTO)*, pp. 1–6, Kobe, Japan, 2018.

[55] X. Xia, X. Zhang, and X. Chen, "Parameter estimation for gaussian mixture processes based on expectation-maximization method," in *2016 4th International Conference on Machinery, Materials and Information Technology Applications*, 2016.

[56] S. Banerjee and M. Agrawal, "On the performance of underwater communication system in noise with Gaussian mixture statistics," in *2014 Twentieth National Conference on Communications (NCC)*, Kanpur, India, 2014.

[57] K. Pelekanakis and M. Chitre, "Adaptive sparse channel estimation under symmetric alpha-stable noise," *IEEE Transactions on Wireless Communications*, vol. 13, no. 6, pp. 3183–3195, 2014.

[58] D. Middleton, *An Introduction to Statistical Communication Theory*, vol. 960, McGraw-Hill New York, 1960.

[59] J. Wang, J. Li, S. Yan et al., "A novel underwater acoustic signal denoising algorithm for Gaussian/non-Gaussian impulsive noise," *IEEE Transactions on Vehicular Technology*, vol. 70, no. 1, pp. 429–445, 2021.

[60] H. Kusao, "Optimum coherent receiver for impulsive rf noise," *Transactions of IEICE Japan*, vol. 68, no. 6, 1985.

[61] S. Mishra and R. R. Tripathi, "Vdhl implementation of Viterbi algorithm for decoding of convolutional code," in *2015 International Conference on Computational Intelligence and Communication Networks (CICN)*, pp. 1367–1370, Jabalpur, India, 2015.

[62] Y. Nakano, D. Umehara, M. Kawai, and Y. Morihiro, "Viterbi decoding for convolutional code over class a noise channel," in *Proceedings of the 7th International Symposium on Power-Line Communications and Its Applications*, pp. 97–102, Kyoto, Japan, 2003.